Nonsinusoidal Current-Phase Relationship in Josephson Junctions from the 3D Topological Insulator HgTe

Ilya Sochnikov,[1,2,*] Luis Maier,[4] Christopher A. Watson,[1,3] John R. Kirtley,[2,3] Charles Gould,[4] Grigory Tkachov,[5] Ewelina M. Hankiewicz,[5] Christoph Brüne,[4] Hartmut Buhmann,[4] Laurens W. Molenkamp,[4] and Kathryn A. Moler[1–3]

[1]*Department of Applied Physics, Stanford University, Stanford, California 94305, USA*
[2]*Geballe Laboratory for Advanced Materials, Stanford University, Stanford, California 94305, USA*
[3]*Stanford Institute for Materials and Energy Sciences, SLAC National Accelerator Laboratory, Menlo Park, California 94025, USA*
[4]*Physikalisches Institut (EP3), University of Würzburg, Am Hubland, 97074 Würzburg, Germany*
[5]*Institute for Theoretical Physics and Astrophysics, University of Würzburg, Am Hubland, 97074 Würzburg, Germany*

(Received 30 September 2014; revised manuscript received 5 December 2014; published 9 February 2015)

We use superconducting quantum interference device microscopy to characterize the current-phase relation (CPR) of Josephson junctions from the three-dimensional topological insulator HgTe (3D HgTe). We find clear skewness in the CPRs of HgTe junctions ranging in length from 200 to 600 nm. The skewness indicates that the Josephson current is predominantly carried by Andreev bound states with high transmittance, and the fact that the skewness persists in junctions that are longer than the mean free path suggests that the effect may be related to the helical nature of the Andreev bound states in the surface of HgTe. These experimental results suggest that the topological properties of the normal state can be inherited by the induced superconducting state, and that 3D HgTe is a promising material for realizing the many exciting proposals that require a topological superconductor.

DOI: 10.1103/PhysRevLett.114.066801 PACS numbers: 73.23.-b, 73.25.+i, 74.45.+c, 74.50.+r

Topological insulators (TIs) have a special band structure with important consequences for proximity-induced superconductivity. In three-dimensional topological insulators (3D TIs), the inversion of the conduction and valence bands leads to conducting 2D surface states with energies that are linearly proportional to their momenta [1–5]. Spin-momentum locking protects the charge carriers at the surface against elastic backscattering [6,7]. These special properties are reflected in the superconducting proximity effect in a superconductor/3D topological insulator (S/3D-TI) bilayer or a superconductor/topological insulator/superconductor (S/TI/S) junction, which may host Majorana quasiparticles in a quasi-1D channel or vortex core [8–10]. Most previous works characterized current-voltage characteristics to determine the critical current's dependence on temperature, gate voltage, or magnetic field [11–22], while a few studies characterized the current-phase relation (CPR) [23,24].

Here, we use a scanning superconducting quantum interference device (SQUID) microscope to perform contactless measurements of the diamagnetic response of Nb/HgTe bilayers and of the CPR of Nb/HgTe/Nb junctions. In contrast to previous CPR results [23,24], we find no evidence for bulk states, and we observe that the CPRs of many junctions of different sizes consistently exhibit forward skewness.

The CPR in a S/TI/S junction is a key diagnostic [8,25–32]. Weak disorder in the TI far from the superconducting contacts theoretically does not affect the induced superconducting state [33,34]; therefore, Andreev bound states should form in high-transmittance surface channels [8,26,27,29,31]. A CPR with forward skewness —that is, a deviation from a perfect sinusoidal form—is a signature of such high-transmittance Andreev bound states [35–37].

To our knowledge, there have not been direct observations of forward skewed CPRs in topological insulators [23,24], although the skewness has been indirectly inferred [24] from the Fraunhofer interference pattern. Previous CPR experiments in topological insulators [23,24] were complicated in part by bulk states, self-inductance effects, and bias voltage, factors that are eliminated in this work.

Moreover, a skewed CPR can also result from ballistic transport [35]. Measurements in metallic break junctions showed that the CPR approaches the predictions for quantum point contacts in the ballistic limit [38]. In metallic atomic point contacts, the CPR was significantly skewed only in contacts with very high transmittance channels [36]. There are reports of skewed current phase relations in graphene [39,40]. A skewed CPR was also observed in Josephson junctions based on a two-dimensional electron gas in semiconducting InAs with an electron mean free path comparable to the junction size [41]. Any observation of a skewed CPR in a S/TI/S junction will thus have to be scrutinized as to the origins of this particular shape.

Unstrained bulk HgTe is a semimetal that is charge neutral when the Fermi energy is at the touching point between the light-hole and heavy-hole bands at the Brillouin zone center [42]. Epitaxial HgTe layers may readily be turned into a topological insulator by inducing strain in the material [42]. In contrast to Bi compounds, such layers exhibit no bulk conductance [42,43]. Our samples are 65-nm-thick HgTe grown by molecular beam epitaxy under coherent strain on a CdTe substrate, leading to a 3D TI with a full gap of ~22 meV.

We measured the CPR in Nb/3D-HgTe/Nb junctions (Fig. 1) using a scanning SQUID microscope. The field coil of the SQUID sensor threads magnetic flux Φ_a through a superconducting ring with a Nb/3D-HgTe/Nb junction; this induces a phase drop $\varphi/2\pi \approx \Phi_a/\Phi_0$ across the junction, where Φ_0 is the superconducting flux quantum (see the Supplemental Material [44] for the description of the calibration procedure). The SQUID sensor detects magnetic flux Φ generated by the total current I in the ring. Both nonscanning [41,55,56]and scanning [23] variations of the present setup have been used in the past. The advantages of the scanning setup include the ability to measure a large number of samples in the same experiment, small parasitic inductances (which allow direct, low-noise measurements of the CPR), and a natural magnetic background signal cancellation in gradiometric SQUIDs [23].

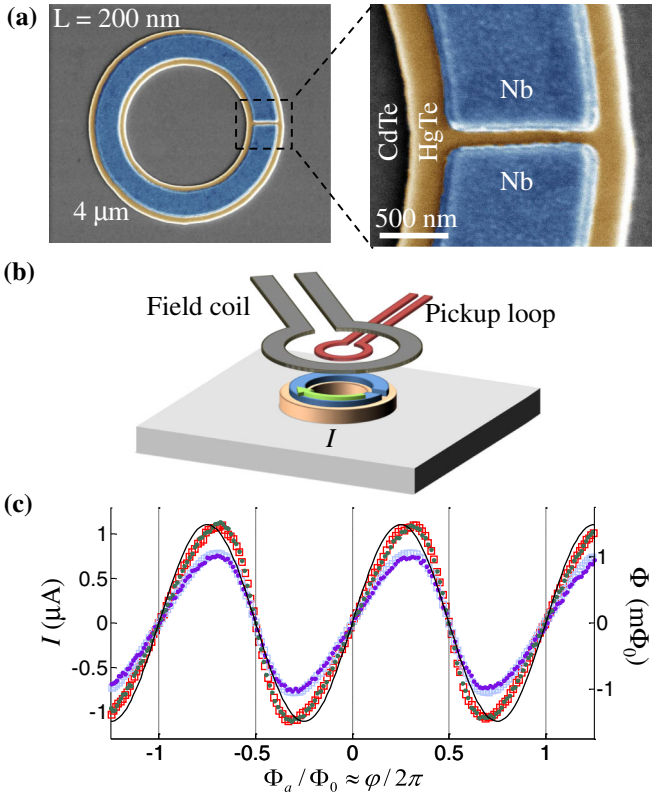

FIG. 1 (color online). Forward skewness in the CPRs of Nb/3D-HgTe/Nb junctions. (a) False-color scanning electron microscopy images of a representative Nb ring with a Nb/3D-HgTe/Nb junction. The separation between the superconducting edges L and width W are 200 and 1000 nm, respectively. (b) Schematic of a CPR measurement. A current applied through the field coil produces an applied flux Φ_a through the sample ring. The applied flux creates a phase drop φ across the junction, inducing a supercurrent I in the ring. The supercurrent modifies the magnetic flux through the pickup loop of the SQUID sensor (red). (c) The CPRs of this junction and three nominally identical ones (colored symbols) exhibit forward skewness, in contrast to a perfectly symmetric sinusoidal form (black solid line).

A typical measured nonsinusoidal CPR at a temperature of 400 mK is shown in Fig. 1(c). In the following text, we refer to the deviation from the sinusoidal form as forward skewness [57]. More specifically, we define the skewness as the amplitude of the second harmonic in the Fourier decomposition of the CPR. Fitting the measured CPR to the functional form $I(\phi) = I_C[\sin(\phi) - A\sin(2\phi)]/\sqrt{1+A^2}$ determines both the skewness A and the critical current I_c (see the Supplemental Material [44]). Note that skewness may also be defined as the phase (modulo 2π) at which the current is maximal; the values of the skewness estimated by these two methods are linearly proportional for small deviations of the CPRs from a perfect sinusoid.

Various inductance effects may lead to the appearance of a skewed CPR. The parameters of our rings imply that they have only a small self-inductance, which concentrates the phase drop across the junctions, ruling out these effects as described in the Supplemental Material [44].

The CPR depends on the junction width W, defined as the superconducting line width [Fig. 2(a)]. Theoretically, the critical current may increase with the number of conducting channels, given by $N = Wk_F/\pi$, where k_F is the Fermi wave vector. Figure 2(b) shows normalized CPRs, highlighting the similarity in the functional form. Figure 2(c) shows that the critical current increases with the width of the junction, consistent with a larger number of conducting channels in wider junctions (see the Supplemental Material [44]). The normalized curves [Fig. 2(b)] and the dependence of the fitted skewness on width [Fig. 2(d)] both demonstrate that skewness is nearly identical for all $L = 200$ nm samples, regardless of width.

We measured the CPR in several junctions of length 200–600 nm [Fig. 3(a)], with the junction length defined as the shortest distance between the superconducting leads. While the amplitude of the periodic CPRs decreased with junction length, the CPRs deviated from a sinusoidal form even for the longest junctions shown in Fig. 3(a). To emphasize this observation, we normalized the curves in Fig. 3(a) by the critical current values [Fig. 3(b)]. The critical current is plotted as a function of the junction length in Fig. 3(c). The observed skewness varied from sample to sample, but persisted even in the longest junctions of 600 nm [Fig. 3(d)].

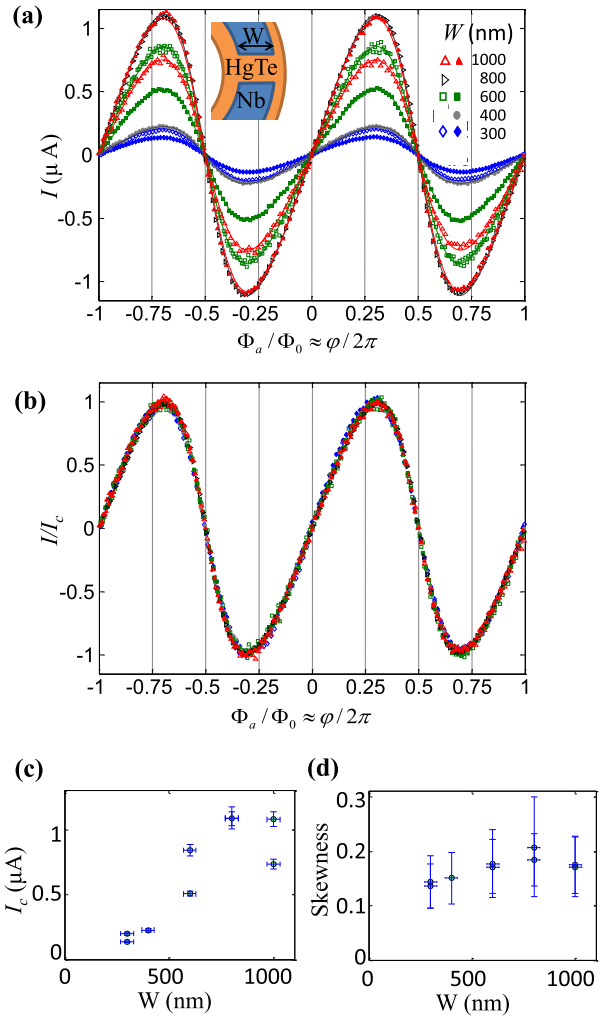

FIG. 2 (color online). Width dependence of the CPR. (a) CPR in Nb/3D-HgTe/Nb junctions with width $W = 300$–1000 nm and $L = 200$ nm, with fits (solid lines) to the S/3D-TI/S model in the text. (b) Data from (a) normalized by the fitted critical current; the same functional form is evident independent of width. (c) Fitted critical current versus junction width for several samples. (d) Fitted skewness versus width. Vertical error bars in (c) and (d) are 68% confidence range of the fits of $I(\phi) = I_C/\sqrt{1+A^2}[\sin(\phi) - A\sin(2\phi)]$ (see text); horizontal error bars are estimates of lithography edge imperfections observed in the SEM images [e.g., Fig. 1(a)]. Skewness does not vary substantially with width.

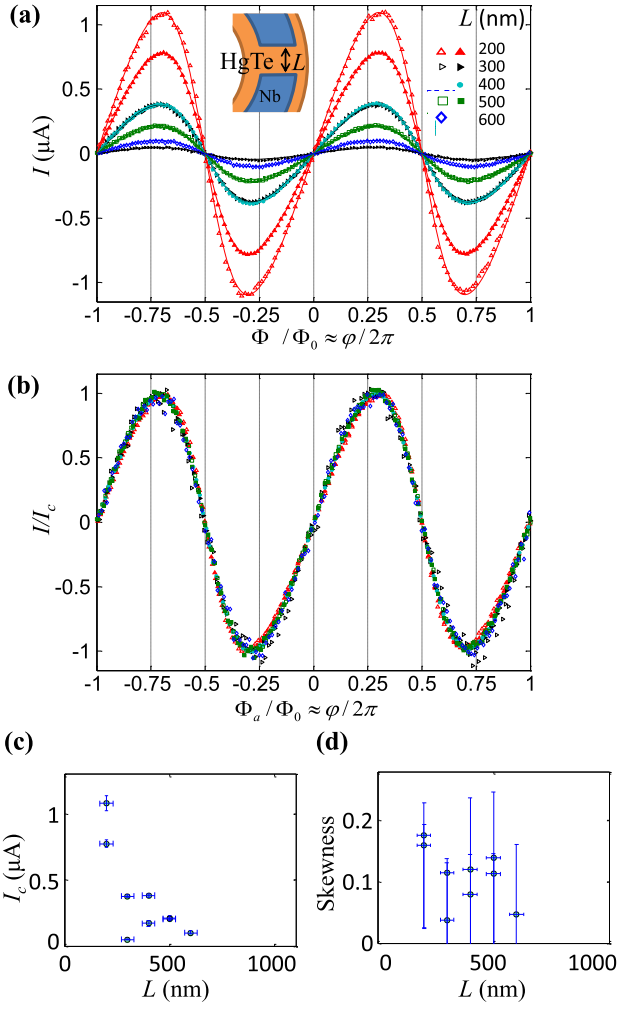

FIG. 3 (color online). Length dependence of the CPR. (a) CPR in Nb/3D-HgTe/Nb junctions with nominal length $L = 200$–600 nm and $W = 1000$ nm. (b) Data from (a) normalized by the fitted critical current. (c) Critical current versus junction length. Skewness (d) versus junction length (solid circles). Vertical error bars in (c) and (d) are 68% confidence range of fits of $I(\phi) = I_C/\sqrt{1+A^2}[\sin(\phi) - A\sin(2\phi)]$ (see text); horizontal error bars are estimates of lithography edge imperfections observed in the SEM images [e.g., Fig. 1(a)]. The skewness persisted even in the longest measured junctions.

To test whether the observed proximity effect primarily occurs at the surface of the 3D HgTe, we measured the magnetic susceptibility of Nb/HgTe and Nb/CdTe bilayers; mesoscopic Nb disks were fabricated on HgTe mesas or the bare, undoped CdTe substrate [Figs. 4(a) and 4(b)]. In previous work, we found that the total magnetic susceptibility of superconducting Al layers fabricated on Bi_2Se_3 was much lower than that of similar Al layers fabricated on bare oxidized silicon [23], indicating that the inverse proximity effect of the bulk states in the Bi_2Se_3 suppressed superconductivity. The bulk of 3D HgTe could potentially be conducting due to dislocations or doping; in the presence of high bulk conduction of the normal layer, the inverse proximity effect is expected to manifest as a suppressed superfluid density of the bilayer [23,58–60]. However, in the absence of bulk conduction, the total superfluid density of a Nb/3D-HgTe bilayer is expected to be close to that of the Nb layer alone. In this case, there is no substantial suppression of the superfluid density due to the inverse proximity effect because the conducting surface layer is very thin compared to the Nb disk. According to this logic, the comparable susceptibility values of Nb/HgTe [Fig. 4(c)] and Nb/CdTe bilayers

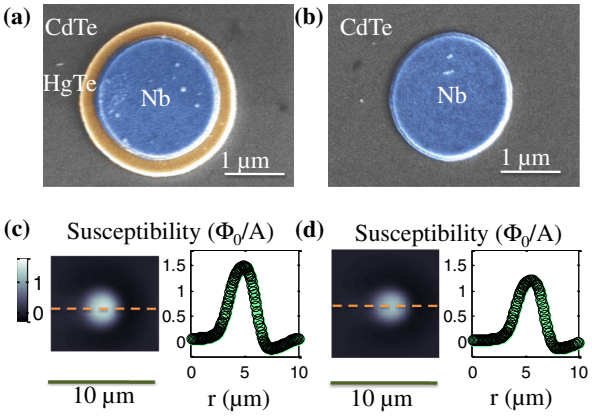

FIG. 4 (color online). Similar values of susceptibility were determined for HgTe/Nb and CdTe/Nb bilayers, showing no evidence of an inverse proximity effect in Nb on HgTe, and supporting the assertion that conducting states are absent in the bulk of the strained HgTe (see text). (a),(b) False-color scanning electron microscopy images of typical Nb disks 2 μm in diameter on (a) a HgTe mesa and (b) CdTe. (c),(d) Representative susceptibility images and cross sections of Nb on (c) HgTe and (d) CdTe. Four additional disk samples were measured, giving similar results (data not shown). Orange dashed lines show the location of the cross sections. Left-to-right skewness of the cross sections is due to the leads and alignment of the SQUID sensor. No evidence for the superfluid density suppression in HgTe/Nb bilayers is found.

[Fig. 4(d)], indicating no suppression of the total superfluid density due to the inverse proximity effect between Nb and strained HgTe, suggest that there is little or no bulk conduction in the HgTe.

In fact, the Nb/HgTe disks appear to have a slightly higher susceptibility compared to Nb/CdTe. This increased susceptibility could be due to the Nb/HgTe structure having a larger total superfluid density, either due to the proximity effect or to surface morphology. However, it could also be due to the fact that the Nb/HgTe disks are slightly closer to the SQUID sensor, by ~100 nm. The Supplemental Material [44] contains the estimated susceptibility at different heights of the SQUID sensor; more detailed modeling and height calibration would be needed to distinguish between these possibilities. The absence of signatures of the possible inverse proximity effect in the superfluid density agrees with the previous observation of an integer quantum Hall effect in the normal state, showing that both the normal and the superconducting conductance of HgTe are dominated by the surface states rather than by bulk states [42].

S/normal metal/S junctions are characterized by the quasiparticle mean free path ℓ and the superconducting coherence length ξ (both of the normal metal region). Theoretical work is simplified for junctions that are either short ($L \ll \xi$) or long ($L \gg \xi$), and for junctions that are either ballistic ($L \ll \ell$) or diffusive ($L \gg \ell$). The clean-limit coherence length is $\xi_0 = \hbar v_F/\pi\Delta$, where $\hbar$ is Planck's constant, v_F is the Fermi velocity in the TI, and Δ is the induced gap. When $\xi_0 \geq \ell$, it is natural to define an effective coherence length ξ, which becomes $\xi \sim (\xi_0 \ell)^{1/2}$ in the limit $\xi_0 \gg \ell$ [35].

Based on parameters determined from transport measurements, junctions with $L = 200$ nm are the best candidates to be in the limit of $\xi, \ell \gtrsim L$. Transport measurements on similar junctions indicate that the phenomenologically determined induced gap is $\Delta \approx 0.1$–$0.2\Delta_{\mathrm{Nb}}$ [12,20], yielding a clean-limit superconducting coherence length $\xi_0 \approx 800$ nm for $\Delta = 0.15$ meV. The quasiparticle mean free path is $\ell \approx 200$ nm, as estimated from normal transport data (see the Supplemental Material [44]).

To model the junctions theoretically, we consider S/3D-TI/S junctions, where the S region describes the surface state of the TI in the proximity with the s-wave superconductor; the 3D TI is treated as a Dirac surface state with a single cone. As shown in Ref. [61], a two-dimensional conducting state under superconducting contacts acts effectively as a two-dimensional superconductor with an induced gap [61]. Therefore, the system in this experiment can be treated as a two-dimensional normal conductor (the HgTe surface between the two Nb leads) making contact with a two-dimensional superconductor with an induced gap (HgTe surface under the Nb contacts). As shown in Ref. [31], theoretically the Josephson current in such junctions is carried by helical Andreev bound states characterized by spin-momentum locking similar to the protected normal state. To determine whether our experimental results can be described within this framework, we extend the previous model [31] to junctions of finite length (but still technically in the short junction limit), and fit the measured CPRs of the $L = 200$ nm junctions. Our fitting procedure allowed for two free parameters: the induced gap Δ and the Fermi wave vector k_F, which together with the width determine the number of conducting channels N.

The data for 200-nm-long junctions are well described by the ballistic junction model with a Dirac surface state, as shown in Fig. 2(a). (The full expression for the theoretical CPR is given in the Supplemental Material [44]). Best-fit values of the induced gap ranged from ~0.12 to ~0.19 meV, consistent with previously reported values in similar HgTe/Nb Josephson junctions [12,20]. Detailed descriptions of the induced gap and number of channels inferred from the fits, together with the fit confidence ranges, are given in the Supplemental Material [44]. The reduction of the fitted gap relative to the Nb gap (~1 meV) has previously been shown to be related to the mismatch of the Fermi surface parameters and the interface transparency [61]. The variability in the fitted gap may be primarily due to differences in the interface transparency. The best-fit number of channels for the $L = 200$ nm junctions agrees with the number of channels calculated using the geometrical width. The superconducting transport through these junctions is thus consistent with what is expected for a

ballistic junction. Moreover, the involved surface states are known to be of a topological origin [20,42]. From the quasiparticle perspective, the forward skewness in the CPR shows qualitatively that highly transmitting Andreev bound states are important contributors to the Josephson current [35]. The quantitative agreement with the model described here (in particular, both the observed skewness and the amplitude of the CPR) supports the interpretation of ballistic quasiparticle transport through helical Andreev bound states [31].

We observed that longer junctions had a reduction in the critical current, but the skewness persisted. Although the theory [31] that we used for the fits may not be strictly applicable for the longer junctions, fits to the CPRs of the longer junctions (see the Supplemental Material [44]) show that the fitted number of channels is reduced with length while the fitted gap is not much changed. This observation indicates that while some channels become ineffective in the formation of Andreev bound states (low transmittance), other channels retain their high transmittance and dominate the transport even in junctions with $L = 600$ nm. Furthermore, the fact that these highly transmitting channels exist in junctions longer than the estimated mean free $\ell \approx 200$ nm path suggests that the scattering in the induced superconducting state is similar to that in the normal state transport and may be influenced by the helical nature of the Andreev bound states in the TI region between the leads (rather than at the TI/S interface).

In summary, we have directly measured CPRs with forward skewness in Nb/3D-HgTe/Nb junctions. The skewness is present in the CPRs of all 16 measured junctions, indicating the importance of highly transmitting Andreev bound states for the superconducting properties of these junctions. Although other models may produce similar skewness, a theoretical model of S/3D-TI/S junctions fits well to the CPRs of the 200-nm-long junctions, suggesting that the helical nature of the Andreev bound states may be important for the suppression of backscattering, similar to the spin-momentum locking in the normal state.

The experimental observation that the induced superconductivity inherits the properties of the topological state in HgTe is an important milestone towards realizing the many exciting theoretical proposals that require a topological superconducting state [3,8–10,62–65]. These results further establish the CPR as an important diagnostic for the basic physics of the Josephson effect in hybrid mesoscopic junctions for fields spanning from superconducting digital electronics to quantum computation.

The work at Stanford University was supported by the Gordon and Betty Moore Foundation through Grant No. GBMF3429. C. A. W., J. R. K., and K. A. M. acknowledge support from the Department of Energy, Office of Basic Energy Sciences, Division of Materials Sciences and Engineering, under Contract No. DE-AC02-76SF00515. E. M. H. acknowledges financial support from the German research foundation (DFG) within FOR1162 (HA5893/5-2). G. T. acknowledges financial support through DFG Grant No. TK60/1-1. The work at EP3 was supported by the DARPA Microsystems Technology Office, MesoDynamic Architecture Program (MESO) through Contract No. N66001-11-1-4105, by the German Research Foundation (DFG Schwerpunkt 1666 "Topological Insulators," the DFG-JST joint research project "Topological Electronics," and the Leibniz program), and the European Research Council Advanced Research Grants (EU ERC-AG) program (Project 3-TOP). I. S. thanks Roni Ilan, Fernando de Juan, Raquel Queiroz, Pavel Ostrovsky, and Martin Leijnse for fruitful discussions.

*ilya.sochnikov@gmail.com

[1] L. Fu, C. L. Kane, and E. J. Mele, Phys. Rev. Lett. **98**, 106803 (2007).
[2] L. Fu and C. L. Kane, Phys. Rev. B **76**, 045302 (2007).
[3] M. Z. Hasan and C. L. Kane, Rev. Mod. Phys. **82**, 3045 (2010).
[4] J. E. Moore and L. Balents, Phys. Rev. B **75**, 121306 (2007).
[5] R. Roy, Phys. Rev. B **79**, 195322 (2009).
[6] H. Beidenkopf, P. Roushan, J. Seo, L. Gorman, I. Drozdov, Y. S. Hor, R. J. Cava, and A. Yazdani, Nat. Phys. **7**, 939 (2011).
[7] P. Roushan, J. Seo, C. V. Parker, Y. S. Hor, D. Hsieh, D. Qian, A. Richardella, M. Z. Hasan, R. J. Cava, and A. Yazdani, Nature (London) **460**, 1106 (2009).
[8] L. Fu and C. L. Kane, Phys. Rev. Lett. **100**, 096407 (2008).
[9] X.-L. Qi and S.-C. Zhang, Rev. Mod. Phys. **83**, 1057 (2011).
[10] C. W. J. Beenakker, Annu. Rev. Condens. Matter Phys. **4**, 113 (2013).
[11] M. Veldhorst, M. Snelder, M. Hoek, T. Gang, V. K. Guduru, X. L. Wang, U. Zeitler, W. G. van der Wiel, A. A. Golubov, H. Hilgenkamp, and A. Brinkman, Nat. Mater. **11**, 417 (2012).
[12] L. Maier, J. B. Oostinga, D. Knott, C. Brüne, P. Virtanen, G. Tkachov, E. M. Hankiewicz, C. Gould, H. Buhmann, and L. W. Molenkamp, Phys. Rev. Lett. **109**, 186806 (2012).
[13] F. Qu, F. Yang, J. Shen, Y. Ding, J. Chen, Z. Ji, G. Liu, J. Fan, X. Jing, C. Yang, and L. Lu, Sci. Rep. **2**, 339 (2011).
[14] B. Sacepe, J. B. Oostinga, J. Li, A. Ubaldini, N. J. G. Couto, E. Giannini, and A. F. Morpurgo, Nat. Commun. **2**, 575 (2011).
[15] J. R. Williams, A. J. Bestwick, P. Gallagher, S. S. Hong, Y. Cui, A. S. Bleich, J. G. Analytis, I. R. Fisher, and D. Goldhaber-Gordon, Phys. Rev. Lett. **109**, 056803 (2012).
[16] F. Yang, F. Qu, J. Shen, Y. Ding, J. Chen, Z. Ji, G. Liu, J. Fan, C. Yang, L. Fu, and L. Lu, Phys. Rev. B **86**, 134504 (2012).
[17] P. Zareapour, A. Hayat, S. Y. F. Zhao, M. Kreshchuk, A. Jain, D. C. Kwok, N. Lee, S.-W. Cheong, Z. Xu, A. Yang, G. D. Gu, S. Jia, R. J. Cava, and K. S. Burch, Nat. Commun. **3**, 1056 (2012).
[18] D. Zhang, J. Wang, A. M. DaSilva, J. S. Lee, H. R. Gutierrez, M. H. W. Chan, J. Jain, and N. Samarth, Phys. Rev. B **84**, 165120 (2011).

[19] S. Cho, B. Dellabetta, A. Yang, J. Schneeloch, Z. Xu, T. Valla, G. Gu, M. J. Gilbert, and N. Mason, Nat. Commun. **4**, 1689 (2012).
[20] J. B. Oostinga, L. Maier, P. Schüffelgen, D. Knott, C. Ames, C. Brüne, G. Tkachov, H. Buhmann, and L. W. Molenkamp, Phys. Rev. X **3**, 021007 (2013).
[21] L. Galletti, S. Charpentier, M. Iavarone, P. Lucignano, D. Massarotti, R. Arpaia, Y. Suzuki, K. Kadowaki, T. Bauch, A. Tagliacozzo, F. Tafuri, and F. Lombardi, Phys. Rev. B **89**, 134512 (2014).
[22] M. Snelder, C. G. Molenaar, Y. Pan, D. Wu, Y. K. Huang, A. d. Visser, A. A. Golubov, W. G. v. d. Wiel, H. Hilgenkamp, M. S. Golden, and A. Brinkman, Supercond. Sci. Technol. **27**, 104001 (2014).
[23] I. Sochnikov, A. J. Bestwick, J. R. Williams, T. M. Lippman, I. R. Fisher, D. Goldhaber-Gordon, J. R. Kirtley, and K. A. Moler, Nano Lett. **13**, 3086 (2013).
[24] C. Kurter, A. D. K. Finck, Y. S. Hor, and D. J. Van Harlingen, arXiv:1307.7764.
[25] L. Fu and C. L. Kane, Phys. Rev. B **79**, 161408 (2009).
[26] A. C. Potter and L. Fu, Phys. Rev. B **88**, 121109 (2013).
[27] M. Snelder, M. Veldhorst, A. A. Golubov, and A. Brinkman, Phys. Rev. B **87**, 104507 (2013).
[28] R. M. Lutchyn, J. D. Sau, and S. Das Sarma Phys. Rev. Lett. **105**, 077001 (2010).
[29] C. T. Olund and E. Zhao, Phys. Rev. B **86**, 214515 (2012).
[30] R. Ilan, J. H. Bardarson, H. S. Sim, and J. E. Moore, New J. Phys. **16**, 053007 (2014).
[31] G. Tkachov and E. M. Hankiewicz, Phys. Rev. B **88**, 075401 (2013).
[32] G. Tkachov and E. M. Hankiewicz, Phys. Status Solidi **250**, 215 (2013).
[33] A. C. Potter and P. A. Lee, Phys. Rev. B **83**, 184520 (2011).
[34] P. A. Ioselevich, P. M. Ostrovsky, and M. V. Feigel'man, Phys. Rev. B **86**, 035441 (2012).
[35] C. W. J. Beenakker, in *Low-Dimensional Electronic Systems*, edited by F. K. G. Bauer and H. Heinrich (Springer-Verlag, Berlin, Heidelberg, 1992).
[36] M. L. Della Rocca, M. Chauvin, B. Huard, H. Pothier, D. Esteve, and C. Urbina, Phys. Rev. Lett. **99**, 127005 (2007).
[37] T. M. Klapwijk, J. Supercond. **17**, 593 (2004).
[38] M. C. Koops, G. V. van Duyneveldt, and R. de Bruyn Ouboter, Phys. Rev. Lett. **77**, 2542 (1996).
[39] C. English, D. Hamilton, C. Chialvo, I. Moraru, N. Mason, and D. Van Harlingen, arXiv:1305.0327.
[40] Ç. Girit, V. Bouchiat, O. Naaman, Y. Zhang, M. F. Crommie, A. Zettl, and I. Siddiqi, Phys. Status Solidi **246**, 2568 (2009).
[41] M. Grajcar, M. Ebel, E. Il'ichev, R. Kürsten, T. Matsuyama, and U. Merkt, Physica (Amsterdam) **372–376C**, 27 (2002).
[42] C. Brüne, C. X. Liu, E. G. Novik, E. M. Hankiewicz, H. Buhmann, Y. L. Chen, X. L. Qi, Z. X. Shen, S. C. Zhang, and L. W. Molenkamp, Phys. Rev. Lett. **106**, 126803 (2011).
[43] J. N. Hancock, J. L. M. van Mechelen, A. B. Kuzmenko, D. van der Marel, C. Brüne, E. G. Novik, G. V. Astakhov, H. Buhmann, and L. W. Molenkamp, Phys. Rev. Lett. **107**, 136803 (2011).
[44] See Supplemental Material at http://link.aps.org/supplemental/10.1103/PhysRevLett.114.066801, which includes Refs. [45–54], for additional data and calculations.
[45] M. Huber, N. Koshnick, H. Bluhm, L. Archuleta, T. Azua, P. Bjornsson, B. Gardner, S. Halloran, E. Lucero, and K. Moler, Rev. Sci. Instrum. **79**, 053704 (2008).
[46] H. Bluhm, N. C. Koshnick, J. A. Bert, M. E. Huber, and K. A. Moler, Phys. Rev. Lett. **102**, 136802 (2009).
[47] N. Koshnick, H. Bluhm, M. Huber, and K. Moler, Science **318**, 1440 (2007).
[48] J. A. Bert, N. C. Koshnick, H. Bluhm, and K. A. Moler, Phys. Rev. B **84**, 134523 (2011).
[49] M. Sigrist and T. Rice, J. Phys. Soc. Jpn. **61**, 4283 (1992).
[50] E. H. Brandt, Phys. Rev. B **72**, 024529 (2005).
[51] A. I. Bobenko and B. A. Springborn, Discrete Comput. Geom. **38**, 740 (2007).
[52] K. Hasselbach, D. Mailly, and J. Kirtley, J. Appl. Phys. **91**, 4432 (2002).
[53] P. Brouwer and C. Beenakker, Chaos Solitons Fractals **8**, 1249 (1997).
[54] C. W. J. Beenakker, D. I. Pikulin, T. Hyart, H. Schomerus, and J. P. Dahlhaus, Phys. Rev. Lett. **110**, 017003 (2013).
[55] L. D. Jackel, R. A. Buhrman, and W. W. Webb, Phys. Rev. B **10**, 2782 (1974).
[56] S. M. Frolov, D. J. Van Harlingen, V. A. Oboznov, V. V. Bolginov, and V. V. Ryazanov, Phys. Rev. B **70**, 144505 (2004).
[57] A. A. Golubov, M. Y. Kupriyanov, and E. Il'ichev, Rev. Mod. Phys. **76**, 411 (2004).
[58] M. Zhang, G. Tateishi, and G. Bergmann, Phys. Rev. B **74**, 014506 (2006).
[59] G. Brammertz, A. Poelaert, A. A. Golubov, P. Verhoeve, A. Peacock, and H. Rogalla, J. Appl. Phys. **90**, 355 (2001).
[60] S. P. Zhao and Q. S. Yang, Phys. Rev. B **59**, 14630 (1999).
[61] A. F. Volkov, P. H. C. Magnée, B. J. van Wees, and T. M. Klapwijk, Physica (Amsterdam) **242C**, 261 (1995).
[62] K. T. Law, P. A. Lee, and T. K. Ng, Phys. Rev. Lett. **103**, 237001 (2009).
[63] Y. Tanaka, T. Yokoyama, and N. Nagaosa, Phys. Rev. Lett. **103**, 107002 (2009).
[64] A. R. Akhmerov, J. Nilsson, and C. W. J. Beenakker, Phys. Rev. Lett. **102**, 216404 (2009).
[65] L. Fu and C. L. Kane, Phys. Rev. Lett. **102**, 216403 (2009).